Available online at www.sciencedirect.com
ScienceDirect
Trans. Nonferrous Met. Soc. China 28(2018) 2151−2161
Transactions of Nonferrous Metals Society of China
www.tnmsc.cn

Microstructures evolution and mechanical properties disparity in 2070 Al−Li alloy with minor Sc addition

Dan-yang LIU[1], Jie-xia WANG[1], Jin-feng LI[1,2]

1. School of Materials Science and Engineering, Central South University, Changsha 410083, China;
2. Science and Technology on High Strength Structural Materials Laboratory, Central South University, Changsha 410083, China

Received 16 September 2017; accepted 3 April 2018

Abstract: The microstructures and mechanical properties of Al−3.35Cu−1.2Li−0.4Mg−0.4Zn−0.3Mn−0.1Zr (mass fraction, %) alloy with Sc addition or free Sc were investigated through tensile test, SEM, EPMA and TEM. The addition of 0.082% (mass fraction) Sc element leads to the formation of Cu-rich and Sc-contained nano-sized $Al_3(ScZr)$ particles and *W* phase particles. The $Al_3(ScZr)$ particles can inhibit recrystallization to a certain extent and impede recrystallized grain growth during solution treatment. It is found that *W* phase cannot dissolve in supersaturated solid solution during the solution heat treatment, and the Cu content in the solutionized matrix is decreased, which causes a decrease in the fraction of Cu-contained strengthening precipitates with T_1 (Al_2CuLi) and θ' (Al_2Cu) under T8 aging condition. Due to the formation of the *W* phases, the small Sc addition causes a little reduction in the strength.

Key words: Al−Li alloy; Sc addition; microstructure; mechanical properties

1 Introduction

The studies on the effect of introducing Sc into Al alloys began in the Soviet Union in 1960s [1]. In order to meet the needs of aerospace industry, a series of Sc-contained Al alloys including Al−Mg alloys and Al−Zn−Mg alloys were developed and investigated. Generally, it is concluded that due to Sc addition, nano-sized coherent Al_3Sc particles precipitate from supersaturated α(Al) matrix during aging treatment or thermo-mechanical processing [2,3], which can strengthen the corresponding Al alloys. Compared to single addition of Sc or Zr, combined addition of Sc and Zr provides better strengthening effect, due to the formation of coherent $Al_3(ScZr)$ dispersoids with $L1_2$ structure [4]. $Al_3(ScZr)$ particles have excellent grain refining effect, which act as heterogeneous nucleation sites during solidification and inhibit re-crystallization effectively [5−9]. They are formed in the Al alloys through the following three approaches: (1) Primary $Al_3(ScZr)$ particles form during solidification [10]. (2) $Al_3(ScZr)$ dispersoids form during homogenization and thermo-mechanical process [11]. (3) Coherent $Al_3(ScZr)$ particles precipitate during aging in the temperature ranging from 250 to 350 °C [12].

For Al−Cu alloys, it was reported that small Sc addition had some negative effects. LEE et al [13] indicated that although minor Sc addition refined the grains, it lowered the tensile strength and hardness of aged Al−4.6Cu−0.3Mg−0.6Ag alloy due to the following two factors. First, the coherent Al_3Sc particles would not precipitate at low aging temperature (below 200 °C in general) applied to the alloy [12]. Second, coarse and indissolvable Al−Cu−Sc ternary phases (*W* phase) with tetragonal crystal structure (a=0.855 nm and c=0.505 nm) formed [4,14,15]. According to the isothermal section of Al-rich corner of the Al−Cu−Sc phase diagram at 500 °C [16,17], the ternary *W* phase forms in the Al−Cu−Sc alloy with Cu content higher than 0.5% (mass fraction), while the amount of Al_3Sc phase is decreased. As the Cu content is increased, Al_3Sc phase will disappear. Although different compositions of the *W* phase, including $Al_{5-8}Cu_{7-4}Sc$, $Al_{5.4-8}Cu_{6.6-4}Sc$ and $Al_{8-x}Cu_{4+x}Sc$, were reported and exhibited distinct properties, it is believed that the effect of *W* phase in Al−Cu alloys was negative [18].

The effects of Sc addition on the mechanical

Corresponding author: Jin-feng LI; Tel: +86-13278861206; E-mail: lijinfeng@csu.edu.cn
DOI: 10.1016/S1003-6326(18)64860-5

properties of Al−Cu−Li alloys with different Cu and Li contents were two-edged. In some Al−Cu−Li alloys with Cu content lower than 2% (mass fraction), such as 8090 and Al−4.0Mg−1.5Cu−1.0Li−0.12Zr alloys, small Sc addition enhanced the strength [19,20]. In some Al−Cu−Li alloys such as 2099 and 1460 alloys with medium Cu content (2.5%−3.5%, mass fraction) and Li content higher than 1.5% (mass fraction), 0.1% Sc (mass fraction) addition also enhanced the strength [21,22]. However, MA et al [22] found that 0.22% (mass fraction) Sc addition led to a slight decrease in the strength of 1460 alloy. In addition, DUTKIEWICZ et al [23] pointed out that 0.2% (mass fraction) Sc addition did not cause strength improving of Al−2.5Li−2.0Cu alloys after ageing at 200 °C. In Al−Cu−Li alloys with high Cu content and low Li content such as 1469 alloy (Al−4.3Cu−1.0Li−0.3Mg−0.4Ag−0.1Zr), only 0.063% (mass fraction) Sc addition caused an obvious decrease in the strength [24].

2050 alloy, a third generation Al−Li alloy, has potential application prospects in aerospace [25−28]. As an alternative to 2050 alloy, 2070 alloy was developed and registered in 2013, which was developed by replacing Ag element in 2050 alloy with Zn element, slightly lowering Cu content and increasing Li content. According to the above literature analysis, small Sc addition provides positive effect on the strength of the alloy with lower Cu content and higher Li content. In addition, compared to 2050 alloy, 2070 alloy possesses this composition feature. Therefore, in this work, minor Sc was added to 2070 alloy and corresponding structures and strength were investigated, to clarify the micro-alloying effect of Sc in this kind of Al−Li alloy.

2 Experimental

2.1 Materials and procedures

The experimental Sc-contained alloy (A) and Sc-free 2070 alloy (B) were designed and prepared. Their chemical compositions are given in Table 1. It should be emphasized that the contents of Cu, Li and Sc were analyzed by inductively coupled plasma optical emission spectrometer (ICP-OES). As for Mg, Zn, Mn and Zr elements, there is minor variation between the designed content and their analyzed content based on our melting and casting practice. Their contents were therefore not analyzed and Table 1 shows their designed contents. The alloy ingots were homogenized at 470 °C for 8 h followed by heating at 520 °C for 24 h. After homogenization, the ingots were rolled into sheets with 2 mm in thickness through hot rolling and cold rolling. After being solution-treated at 525 °C for 1 h followed by quenching in water, the samples were subjected to a T8 temper (aging for different time at 155 °C after 6% pre-deformation through cold rolling).

Table 1 Chemical compositions of studied alloys (mass fraction, %)

Alloy	Cu	Li	Mg	Zn	Mn	Sc	Zr	Al
A	3.36	1.19	0.4	0.4	0.3	0.082	0.1	Bal.
B	3.34	1.16	0.4	0.4	0.3	−	0.1	Bal.

2.2 Tensile tests

Test samples with a parallel section gauged 30 mm in length and 8 mm in width were cut from the sheets. Yield strength (YS), ultimate tensile strength (UTS) and elongation of the samples were measured using the MTS 858 universal testing machine with a strain rate of 1.0×10^{-3} mm/s at ambient temperature. Three tensile tests were carried out for each condition, and the average strength and elongation were then calculated.

2.3 Structure observation

Secondary phases in the as-cast, homogenized and aged samples were observed through an FEI Quanta 650 FEG scanning electron microscope (SEM) in the backscattered electron (BSE) mode, and their constituent elements were analyzed through energy dispersive X-ray spectroscopy (EDS) equipped with SEM. Particle composition was mainly determined through electron probe microanalysis (EPMA) (JXA−8800R, JEOL, Japan) equipped with an OXFORD INCA 500 wave dispersive X-ray spectrometer (WDS).

The samples for metallographical observations were mechanically ground and polished, washed ultrasonically with ethanol, and then anodically treated at 24 V in a solution containing 1.1 g H_3BO_3, 95 mL H_2O and 3 mL HF. The metallographical observations were performed with an optical microscopy (OM, Leica DMI300 M).

Precipitates were observed through transmission electron microscopy (TEM). The TEM samples were prepared by mechanical grinding and twin-jet electropolishing in a solution containing 30% nitric acid and 70% methanol (volume fraction) at −25 °C with a voltage of 15−20 V. TEM observation was performed with a Tecnai $G^2$20 microscope operating at 200 kV through conventional bright-field (BF), dark-field (DF) imaging, and selected area electron diffraction (SAED).

3 Results

3.1 As-cast and homogenized structures

Figure 1 shows the OM and BSE images of the as-cast Sc-contained alloy A and Sc-free alloy B. Both alloys consist of typical large and dendritic grains. The

average grain size is 350−450 μm for Sc-contained alloy A (Fig. 1(a)) and about 400−500 μm for Sc-free alloy B (Fig. 1(b)). There is insignificant decrease in the grain size caused by 0.082% Sc addition. In the BSE images, a large number of white net-like non-equilibrium phases are observed along dendrite (Figs. 1(c, d)). In addition, in the Sc-contained as-cast alloy A, it seems that more significant micro-segregation is observed within the grains, which may act as the heterogeneous nucleus to the *W* phase or primary $Al_3(ScZr)$ particles.

The OM images and BSE images of homogenized Sc-contained alloy A and Sc-free alloy B are shown in Fig. 2. After homogenization, the dendritic grain structures almost disappear (Fig. 2(b)). The grain of the Sc-contained alloy A is a little smaller than that of Sc-free alloy B. Meanwhile, there only exist some discontinuous small particles (Figs. 2(c, d)), indicating that most continuous no-equilibrium phases are dissolved. In addition, it is more important that the amount of residual particles in the Sc-contained alloy A (Fig. 2(c)) is much more than that in the Sc-free alloy B (Fig. 2(d)).

Figure 3 shows the EDS analysis of the particles in the as-cast Sc-contained alloy A. In addition to the non-equilibrium phases of θ' (Al_2Cu) and S' (Al_2CuMg) (figure omitted), there also exist some secondary phases consisting of Al, Cu and Sc elements (Figs. 3(a, b)).

Figure 4 shows the elemental mappings of Cu, Mg, Mn, Zr and Sc in a certain area of Sc-contained alloy A and Sc-free alloy B characterized by EPMA. Li element is hard to be detected. After homogenization, in the Sc-free alloy B, there exist a few residual particles segregated by Cu and Mn atoms. Mg almost dissolves into the Al matrix, indicating that homogenization treatment successfully avoids the micro-segregation of Mg atoms. It is reasonable to believe that the residual particles mainly are refractory Al(CuMn) phases, which have high melting point.

There are more residual particles in the Sc-contained alloy A. In addition to Al(CuMn) particles, there exist some other particles. It is found that Cu, Sc and Zr elements tend to concentrate together in some particles. Note that the color of Zr in the element mapping is slight, and that of Cu and Sc is bright. It is obvious that these residual particles mainly contain Al, Cu and Sc elements and a small percentage of Zr. In addition, the area containing Cu and Sc atoms is larger than that containing Cu and Mn atoms.

In both homogenized alloys, Mg atoms are evenly distributed (Fig. 4(e)), which indicates that the homogenization treatment has successfully eliminated the micro-segregation of Mg. In contrast, in the Sc-contained alloy A, the element mapping of Sc shown in Fig. 4(f_1) illustrates that Sc segregation in the array of

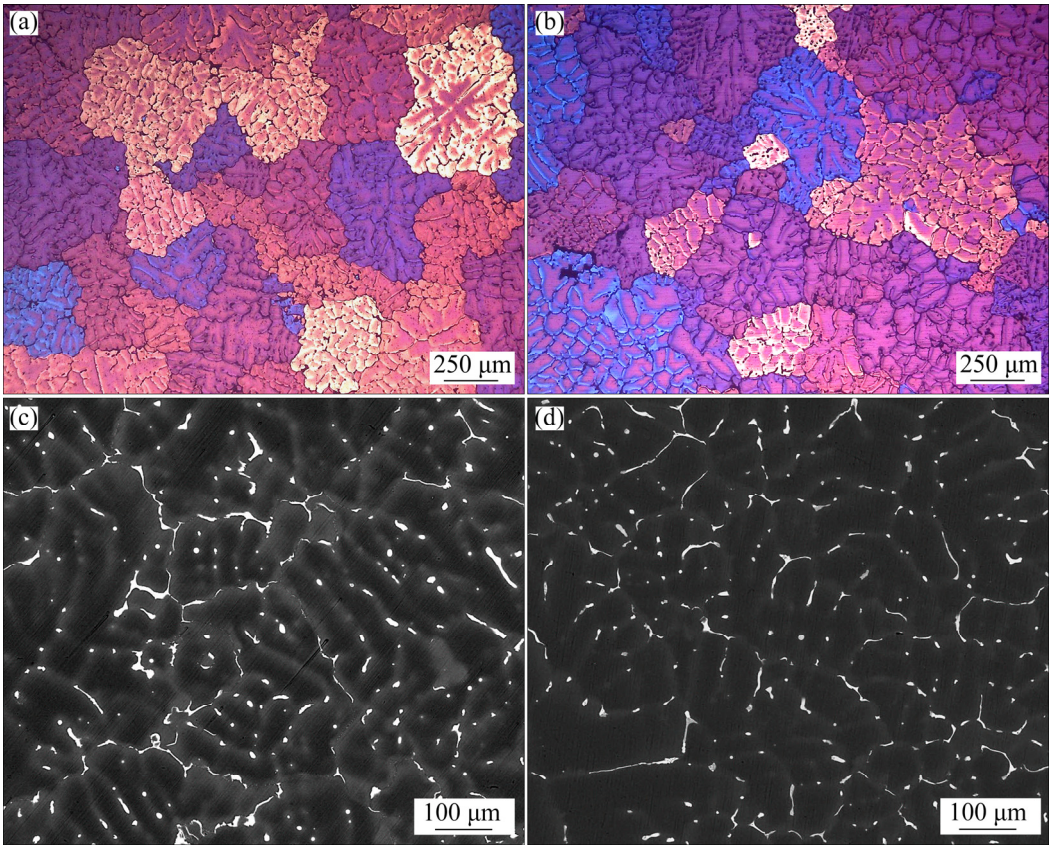

Fig. 1 OM images (a, b) and BSE images (c, d) of as-cast alloys: (a, c) Sc-contained alloy A; (b, d) Sc-free alloy B

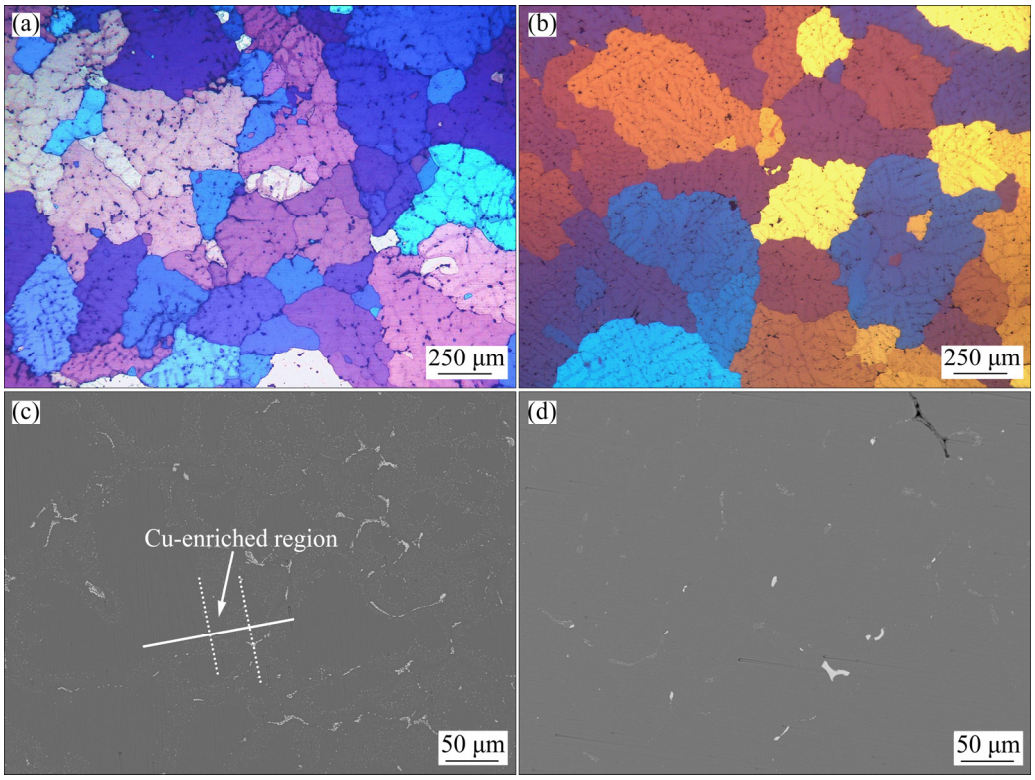

Fig. 2 OM images (a, b) and BSE images (c, d) of homogenized alloys: (a, c) Sc-contained alloy A; (b, d) Sc-free alloy B

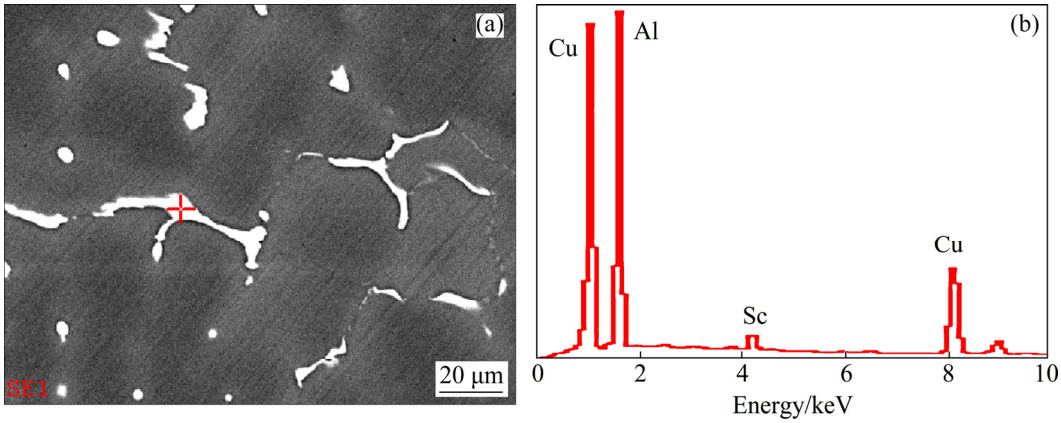

Fig. 3 BSE image (a) and EDS analysis result of particle (b) in as-cast Sc-contained alloy A

the round particles forms after homogenization. Zr element mapping displays the same segregation feature (Fig. 4(c)). It is worth mentioning that the Zr atoms gather together in the white round particles intensively after the addition of Sc. This indicates that Sc segregation tends to attract Zr atoms.

Note that the color scale ranges of the two pictures in Fig. 4(b) are slightly different. The color of Cu atoms in the element mapping is light blue in the Sc-free alloy B (Fig. 4(b_2)). However, Cu atoms exhibit two colors in the element mapping of the Sc-contained alloy A (Fig. 4(b_1)). One is bright in the particles, and the other is deep blue in the Al matrix. Meanwhile, it is observed that the color scale range showing Sc distribution (Fig. 4(f_1)) is much similar to that showing Cu distribution. This Cu mapping demonstrates that Cu atoms are dissolved more completely and distributed evenly in the Sc-free alloy B. On the contrary, the Cu atoms in the Al matrix of the Sc-contained alloy A may be insufficient during the subsequent aging process.

EPMA was used to verify the compositions of various residual particles in the homogenized Sc-contained alloy A. Along the line across the coarse particles in Fig. 4(a_1), the composition profiles detected by EPMA are illustrated in Fig. 5. In addition to Al, small Sc content and high Cu content are detected in the coarse particles. This indicates that the coarse particles are Cu-enriched and Sc-contained ones.

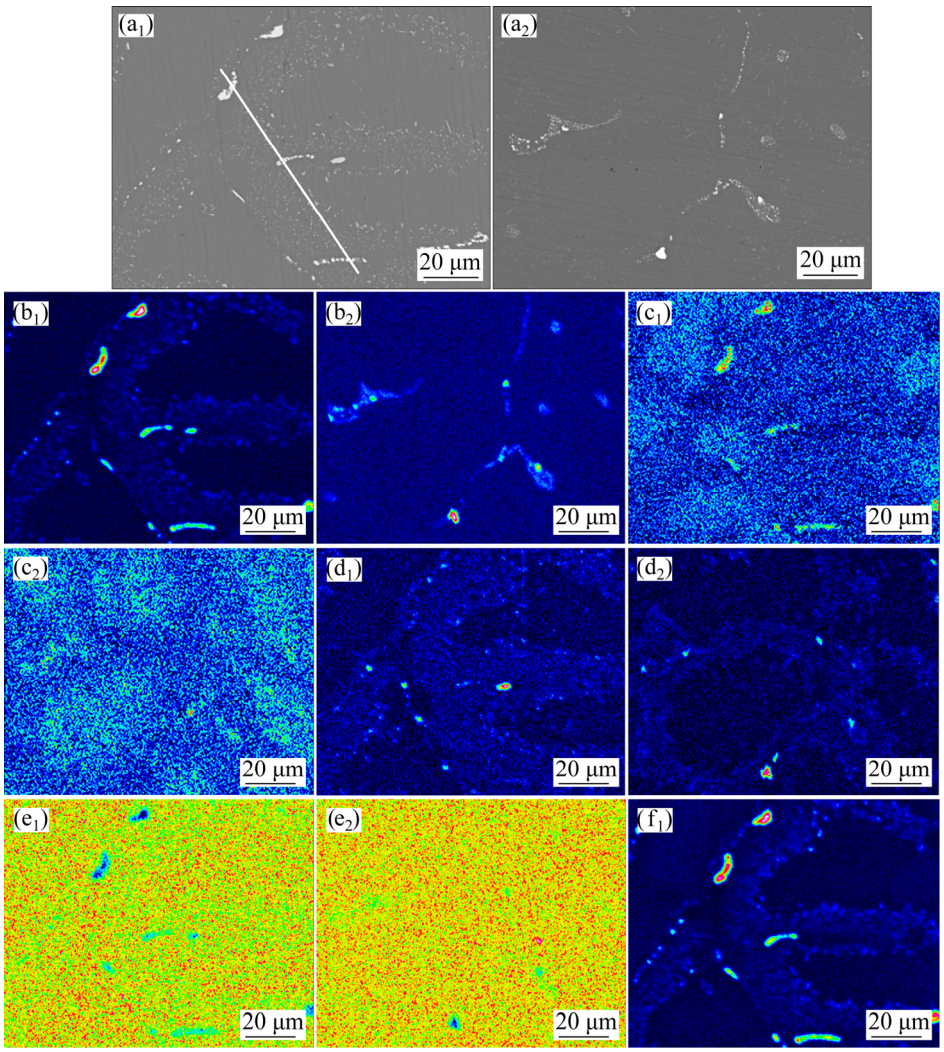

Fig. 4 BSE images (a) and Cu (b), Zr (c), Mn (d), Mg (e) and Sc (f) element mappings of selected area in homogenized alloys: (a_1−f_1) Sc-contained alloy A; (a_2−e_2) Sc-free alloy B

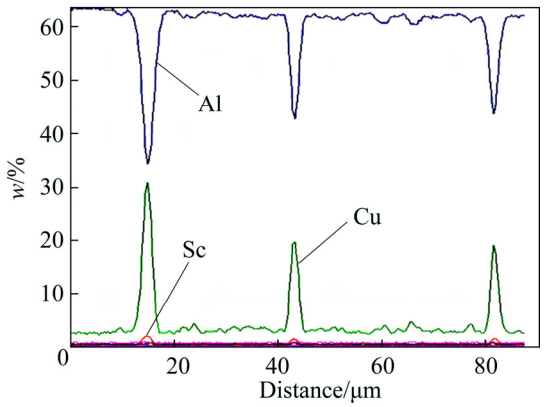

Fig. 5 Content profile detected by EPMA along line across coarse particles in Sc-contained alloy A shown in Fig. 4(a_1)

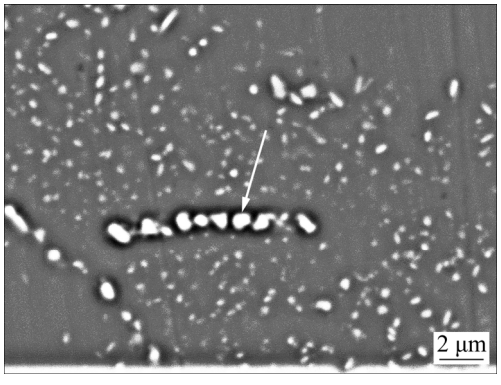

Fig. 6 BSE image of homogenized Sc-contained alloy A

The WDS was used to analyze compositions of the round residual particle marked with an arrow in Fig. 6. The detected composition is listed in Table 2, which is in accordance with the result of line scanning in Fig. 5. The contents of Cu and Sc in the particle are 34.6% and 2.0% (mass fraction), respectively, which are much higher than the average contents of Cu and Sc in the Sc-contained alloy A. The above analyses indicate that as 0.082% Sc is added to 2070 alloy, Cu-enriched and Sc-contained particles are formed during the solidification process and

unable to dissolve into the matrix during the homogenization process.

Table 2 WDS analysis results of particle under EPMA condition in Fig. 6 (mass fraction, %)

Al	Cu	Mg	Zn	Mn	Zr	Sc	Fe
61.8	34.6	0.36	0.34	0.46	0.41	2.00	0.06

It is noteworthy that the nano-sized $Al_3(ScZr)$ particles are formed in the Sc-contained alloy A after homogenization. Figure 7 shows the $[100]_{Al}$ SAED pattern and TEM BF image of the Sc-contained alloy A after homogenization followed by air cooling. Weak spots appear at $\{110\}_{Al}$ and $\{100\}_{Al}$ in the SAED pattern (Fig. 7(a)), indicating that $Al_3(ScZr)$ particles are possibly formed. BF image viewed along $\langle 100\rangle_{Al}$ direction confirms their formation (Fig. 7(b)).

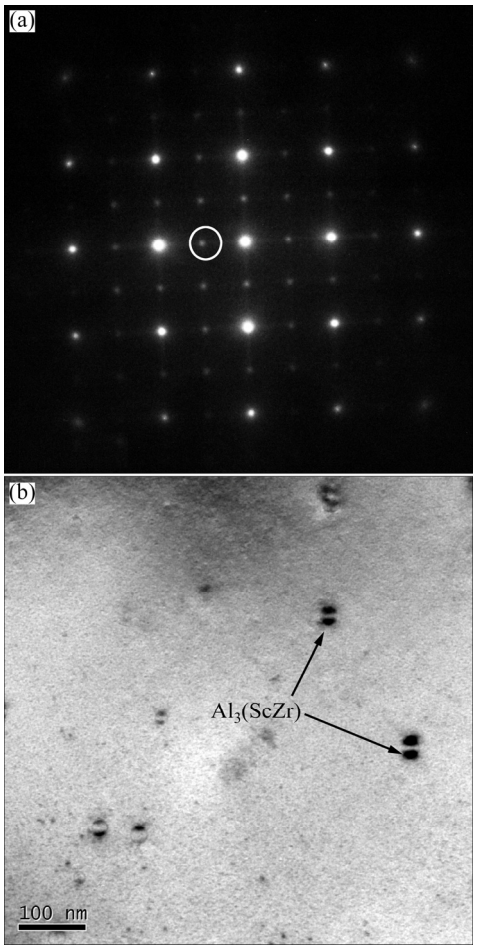

Fig. 7 $[100]_{Al}$ SAED pattern (a) and TEM BF image (b) of Sc-contained alloy A viewed along $\langle 100\rangle_{Al}$ direction after homogenization followed by air cooling

3.2 Structures after solution and aging treatment

Figure 8 shows the OM images of 0.082% Sc-contained and Sc-free alloys after solution treatment. In 0.082% Sc-contained alloy A, some grains show un-recrystallized feature with fiber-like grain structures (Fig. 8(a)). Complete re-crystallization occurs in the Sc-free alloy B, which is characterized by equiaxed grains (Fig. 8(b)). In addition, the recrystallized grain size of the Sc-contained alloy A is a little smaller than that of the Sc-free alloy B.

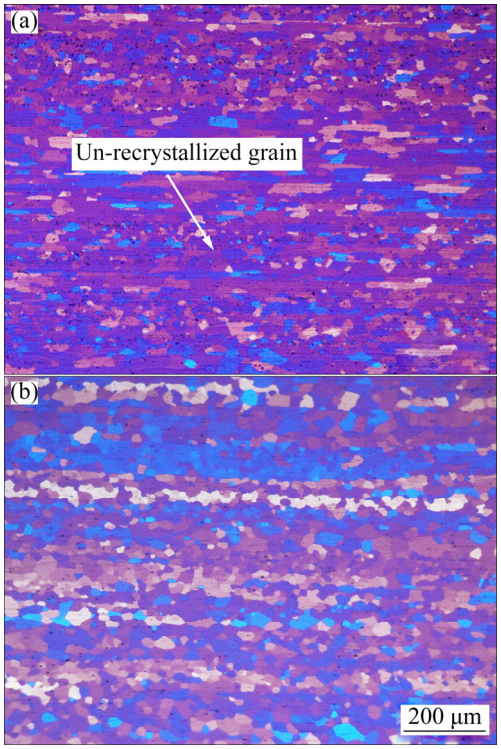

Fig. 8 OM images of 0.082% Sc-contained alloy A (a) and Sc-free alloy B (b) after solution treatment

After T8 peak-aging following solution treatment, the SAED patterns taken from $[112]_{Al}$ and $[100]_{Al}$ zone axes and DF images viewed along $\langle 112\rangle_{Al}$ and $\langle 100\rangle_{Al}$ directions are shown in Fig. 9. For the Sc-contained alloy A, the spots of T_1 and S' (Al_2CuMg) precipitates appear in the $[112]_{Al}$ SAED pattern, and a number of T_1 and some S' precipitates can be observed in the DF image (Fig. 9(a)). In the $[100]_{Al}$ SAED pattern, the spots of θ' are observed, and many θ' phases are detected in the DF image viewed along the $\langle 100\rangle_{Al}$ direction, as shown in Fig. 9(b). Meanwhile, some $Al_3(ScZr)$ particles are observed (Fig. 9(b)), which already exist in the homogenized condition (Fig. 7(b)). Figure 9(c) shows the $[112]_{Al}$ SAED pattern and DF image of the Sc-free alloy B viewed along $\langle 112\rangle_{Al}$ direction. It is indicated that there are more plate-shaped T_1 precipitates but less S' precipitates in the Sc-free alloy B than in the Sc-contained alloy A. The DF image viewed along the $\langle 100\rangle_{Al}$ direction suggests that there are more θ' precipitates in the Sc-free alloy B (Fig. 9(d)). In general, it seems that the number and diameter of T_1 and θ' in the Sc-contained alloy A are smaller than those in the Sc-free alloy B.

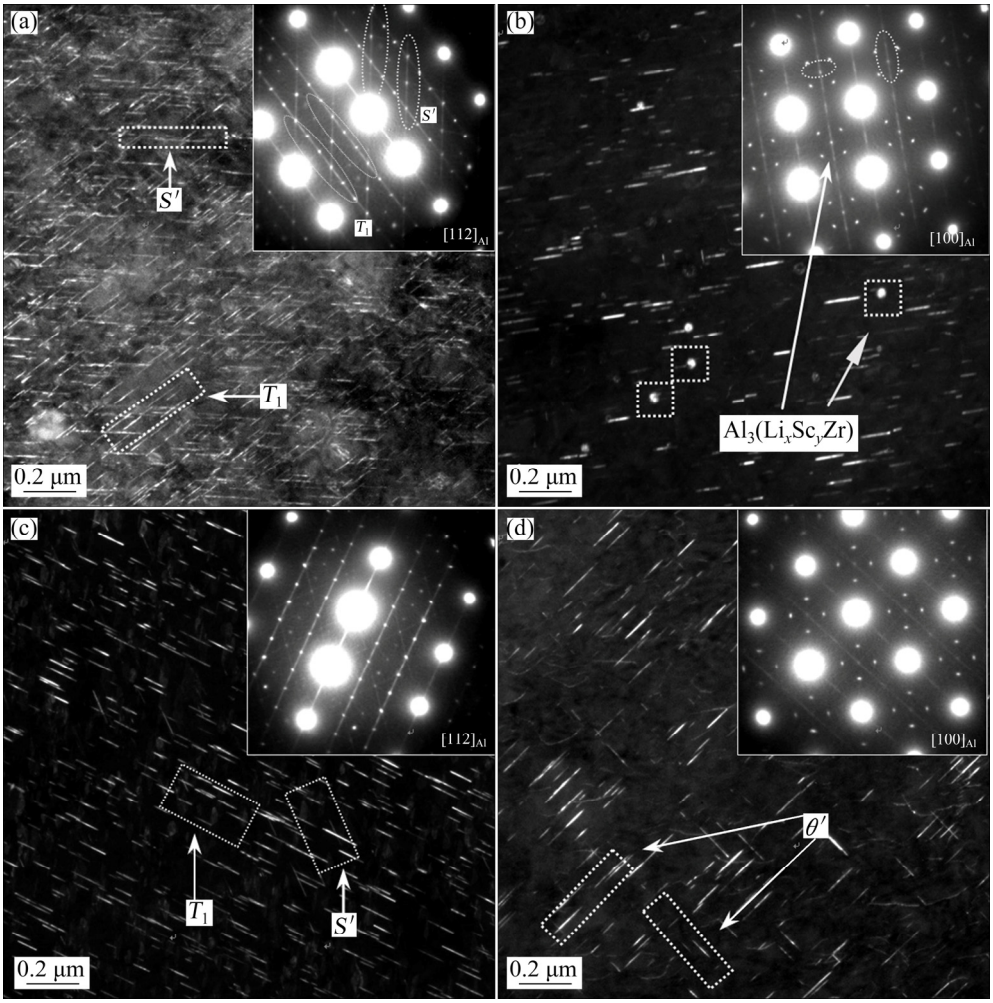

Fig. 9 SAED patterns and TEM images of T8 peak-aged Sc-contained alloy A (a, b) and Sc-free alloy B (c, d): (a, c) DF images viewed along $\langle 112\rangle_{Al}$ direction; (b, d) DF images viewed along $\langle 100\rangle_{Al}$ direction (Inserts in Fig. 9(a, c) show $[100]_{Al}$ SAED patterns and those in Fig. 9(b, d) show $[112]_{Al}$ SAED patterns)

3.3 Tensile properties

Figure 10 demonstrates the tensile property evolution of the studied alloys as a function of T8 aging time. The strength of both the Sc-contained alloy A and the Sc-free alloy B firstly increases to a peak value with the extension of aging time, and then it remains relatively stable during the following 120 h of aging time. The elongation of both alloys decreases quickly with aging time extension. After peak-aging, there is only a very small decrease in the elongation.

It is of interest that the strength of the Sc-contained alloy A is slightly lower than that of the Sc-free alloy B. In Al−Cu−Li alloys, the strength is dependent on the total mole fraction of Cu and Li and their mole ratio. According to our previous investigations [29,30], if no Sc is added, the Cu and Li content characteristics determine that the strength of the alloy A should be a little higher than that of the alloy B. The decrease in the strength of the Sc-contained alloy A in this case is therefore caused by the addition of 0.082% Sc.

4 Discussion

Sc elements added to Al alloys may exist in three forms after the non-equilibrium freezing process. First, some Sc atoms dissolve into α(Al) matrix; Second, a part of Sc atoms exist as primary Al_3Sc particles; Third, some other Sc atoms form Cu-rich and Sc-contained particles. Significant grain refining effect of Sc addition in Al alloys has been reported in many studies [31]. The crystal lattice of Al_3Sc (a=0.4103 nm) [32] is similar to that of the α(Al) matrix (a=0.4049 nm). Therefore, the primary Al_3Sc particles can act as nuclei for Al solidification [33]. However, it is known that the solid solubility of Sc in pure Al at 640 °C is about 0.31% (0.186% in mole fraction), which is much higher than 0.082% of the added Sc in the alloy A. This indicates that primary Al_3Sc particles barely form in the 0.082% Sc-contained alloy A during solidification. The as-cast structure is therefore not obviously refined, which still appears as large dendritic grain structure (Fig. 1).

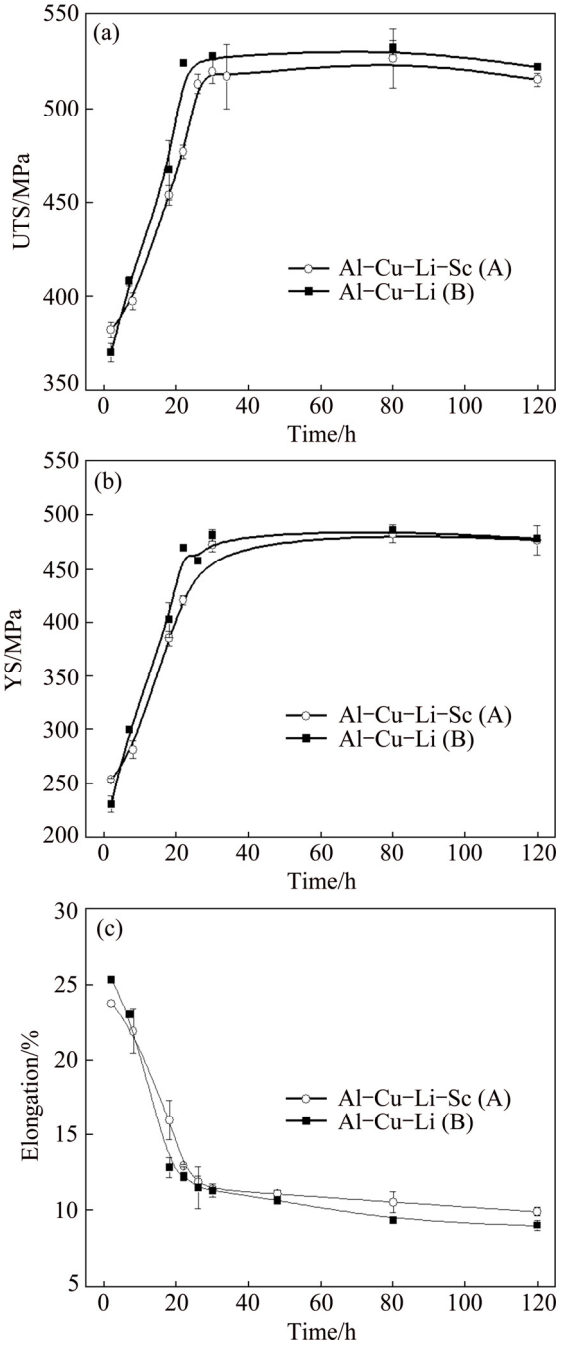

Fig. 10 Tensile properties of Sc-contained alloy A and Sc-free alloy B as function of T8 aging time at 155 °C: (a) Ultimate tensile strength; (b) Yield strength; (c) Elongation

The solid solubility of Sc in pure Al will be decreased as temperature is lowered. It was reported that it was decreased from 0.31% (0.186% in mole fraction) at 640 °C to 0.055% (0.033% in mole fraction) at 470 °C, and it was further decreased in Al−Cu−Sc alloy. During the homogenization process at 470−520 °C and hot rolling process, the Sc atoms combine with Zr atoms to form nano-sized $Al_3(ScZr)$ particles (Fig. 7). The $Al_3(ScZr)$ particles are coherent with the matrix and dispersedly distributed. In addition, they can retard the migration of grain boundaries. The existence of some un-recrystalized grains and smaller recrystallized grain size (Fig. 8) in the solutionized 0.082% Sc-contained alloy A should be associated with the formation of these $Al_3(ScZr)$ particles. Furthermore, these particles can also pin the dislocation to reinforce the alloy.

Cu-rich and Sc-contained particles are observed in the homogenized alloy A (Figs. 4, 5 and 6), which are defined as the *W* phases. Some of them are formed during the solidification process (Figs. 3(a, b)), and the others should be formed during the homogenization process. According to the Al−Cu−Sc ternary phase diagram under the equilibrium state [34], the *W* phases can be formed in this 0.082% Sc-contained alloy A with 3.36% Cu. JIA et al [10] and GAZIZOV et al [17] also claimed that AlCu phases that formed during solidification acted as the precursors and transformed in to the *W* phases during the homogenization process by consuming the Sc atoms in the supersaturated solid solution. In addition, BO et al [35] assessed the Al-rich corner in Al−Cu−Sc system thermodynamically, calculating that the reaction (Liquid + $Al_3Sc \rightleftharpoons$ *W*(AlCuSc) + α(Al)) occur under equilibrium state. This reaction indicates that the *W* phase has a lower Gibbs energy than Al_3Sc, and shows a high level of thermodynamic stability during heat treatment. The above observations and literature analysis indicate that the *W* phases in the Sc-contained alloy A can be formed during both the solidification process and homogenization process. Once they are formed, the *W* phases are difficult to dissolve into the matrix and can exist throughout thermo-mechanical treatments. In this 0.082% Sc-contained alloy A, the formed *W* phases still exist as residual particles after solution treatment at 525 °C and aging, as shown in Fig. 11. After T8 aging following deformation process and solution treatment, considerable residual particles are found (Fig. 11(a)). EDS analysis shows that they are Cu-enriched and Sc-contained particles (Fig. 11(b)), similar to the composition of the particles in the homogenized structure [36,37].

The formation of the *W* phases can cause a decrease of Cu content in the solutionized matrix. The Cu-contained precipitates of T_1 and θ' are originated from the solutionized matrix, so 0.082% Sc addition affects their fraction. Table 3 summarizes the average population densities and diameters of the major precipitates (Fig. 9) in these two alloys with T8 peak-aging. For an accurate detection, at least three DF images are used. The number densities of T_1 and θ' precipitates in the Sc-contained alloy A are 140 and 53 μm^{-2}, respectively. However, in the Sc-free alloy B, the number densities of both T_1 (179 μm^{-2}) and

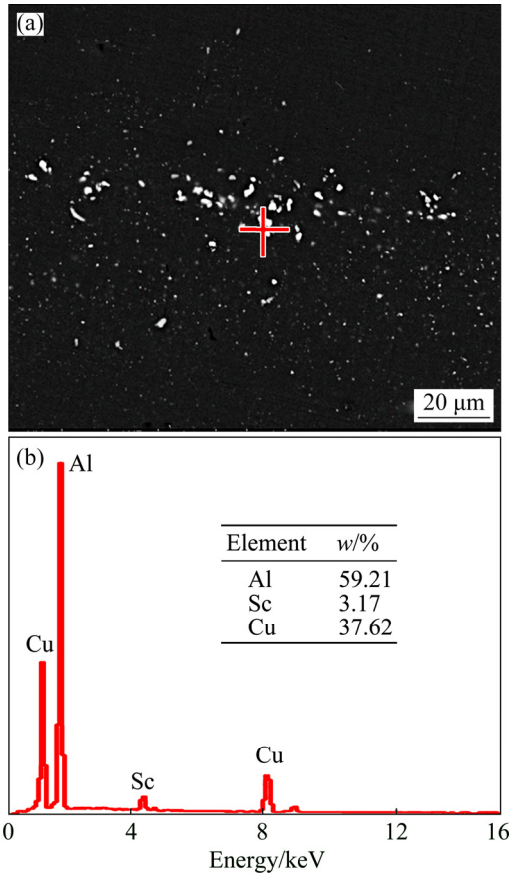

Fig. 11 BSE image (a) and EDS analysis result of residual particle (b) of aged 0.082% Sc-contained alloy A

Table 3 Number density and size of major precipitates in T8 peak-aged alloys

Precipitate type	Statistical source	Alloy	Number density/ μm^{-2}	Diameter/ nm	Length/ nm
T_1	DF images along $\langle 112\rangle_{Al}$ direction	A	140	20−160	
		B	179	20−190	
θ'	DF images along $\langle 100\rangle_{Al}$ direction	A	53		20−240
		B	77		20−240
S'	DF images along $\langle 112\rangle_{Al}$ direction	A	36	20−130	
		B	11	20−120	

θ' (77 μm^{-2}) are higher. In addition, the length of T_1 precipitates in the Sc-free alloy B is a little larger than that in the 0.082% Sc-contained alloy A. These indicate that 0.082% Sc addition decreases the fraction of T_1 and θ' precipitates in the T8 peak-aged alloy, which could lead to a strength lowering of the Sc-contained alloy A.

On the other hand, the addition of 0.082% Sc increases the amount of rod-like S' phase precipitates, which has smaller strengthening effect than T_1 and θ' precipitates. Meanwhile, $Al_3(ScZr)$ particles form during homogenization, which can enhance the strength through precipitation strengthening and substructure strengthening [38]. The synergetic effect, including negative effect on strength by T_1 and θ' precipitates decreasing and positive effect on strength by $Al_3(ScZr)$ particles, causes only a small decrease in the strength of the 0.082% Sc-contained alloy A.

The above analysis illustrates that if an Al−Cu−Li alloy such as 2070 is mainly strengthened by Cu-contained precipitates of T_1 and θ', its strength will be lowered by small Sc addition. However, the strengthening precipitate types of Al−Cu−Li alloys are dependent on Cu/Li ratio. The main possible precipitates include δ' (Al_3Li), $\delta'+T_1$ or $T_1+\theta'$ in Al−Cu−Li alloys with different Cu/Li ratio [29,30]. Based on this consideration, the effect of Sc addition in Al−Cu−Li alloys should be related to the Cu/Li ratio. In the Al−Cu−Li alloys such as 1469 alloy with high Cu content and high Cu/Li ratio, the main precipitates are T_1 and θ'. The addition of small Sc leads to a decrease in the strength, due to the formation of the W phases [10,24]. In other words, small Sc addition shows negative effect on the strength of the Al−Cu−Li alloys with high Cu content and high Cu/Li ratio. In the Al−Cu−Li alloys with Cu/Li ratio lower than 2.0, the main strengthening precipitates are δ'. There only exists a small number of T_1, and small Sc addition shows different effect on the strength. ZHANG et al [21] and SHI et al [39] indicated that in both 2099 alloy with a Cu/Li ratio of 1.64 and Al−3Li−1.5Cu−0.15Zr cast alloy with a Cu/Li ratio of 0.5, the most important aging precipitates were δ', and the fraction of T_1 was much smaller than that of δ'. Accordingly, 0.1% Sc and 0.15% Sc enhanced their strength, respectively. In Al−3.0Cu−2.0Li−0.12Zr alloy strengthened by a large number of δ' precipitates and some T_1 precipitates, 0.11% Sc addition (i.e., 1460 alloy) was also found to enhance the strength, though Cu-rich and Sc-contained W phases were possibly formed. In these three alloys, a crucial factor for the strength enhancement was correlated to the formation of $Al_3(ScZr)$ or $Al_3Li/Al_3(ScZr)$ particles due to the small addition of Sc. However, in 1460 alloy, as the Sc addition was further increased to 0.22%, the strength was lowered. A possible explanation for this phenomenon may be associated with the fact that the strength enhancement by $Al_3(ScZr)$ particles cannot match the strength reduction caused by T_1 content decreasing due to the formation of more Cu-rich and Sc-contained W phases.

By combining this work and literature analysis, it is suggested that the strength enhancement by Sc addition is mainly suitable for some Al−Cu−Li alloys. In the alloys mainly strengthened by T_1 and θ' precipitates, the small addition of Sc may display a negative effect on the strength.

5 Conclusions

1) The small Sc addition leads to the formation of two phases: the nano-sized $Al_3(ScZr)$ particles precipitated during homogenization process, and the Cu-rich and Sc-contained W phases formed during solidification process and homogenization process.

2) The small Sc addition does not display grain refining effect on the cast structure. However, the nano-sized $Al_3(ScZr)$ particles formed during homogenization process inhibits recrystallization to a certain extent and retard the recrystallized grain growth during the solution treatment.

3) The W phases exist as residual particles in the solutionized alloy, which decreases the Cu content in the solutionized matrix and therefore the fraction of Cu-contained phases of T_1 and θ' precipitated during the following aging process.

4) The strength of the alloy is lowered a little by the small Sc addition to form copper-contained W phase, which reduces the amount of main precipitation phase of T_1 phase and θ' phase in the aged condition.

References

[1] DAVYDOV V G, ROSTOVA T D, ZAKHAROV V V, FILATOV Y A, YELAGIN V I. Scientific principles of making an alloying addition of scandium to aluminium alloys [J]. Materials Science and Engineering A, 2000, 280: 30−36.

[2] STOCK H R, KOEHLER B, BOMAS H, ZOCH H W. Characteristics of aluminium−scandium alloy thin sheets obtained by physical vapour deposition [J]. Materials and Design, 2010, 31(S): s76−s81.

[3] APPS P J, BERTA M, PRANGNELL P B. The effect of dispersoids on the grain refinement mechanisms during deformation of aluminium alloys to ultra-high strains [J]. Acta Materialia, 2005, 53: 499−511.

[4] RIDDLE Y W, SANDERS T H. A study of coarsening, recrystallization, and morphology of microstructure in Al−Sc−(Zr) −(Mg) alloys [J]. Metallurgical and Materials Transactions A, 2004, 35A: 341−350.

[5] BOOTH-MORRISON C, DUNAND D C, SEIDMAN D N. Coarsening resistance at 400 degrees C of precipitation-strengthened Al−Zr−Sc−Er alloys [J]. Acta Materialia, 2011, 59: 7029−7042.

[6] DEV S, STUART A A, KUMAAR R C R D, MURTY B S, RAO K P. Effect of scandium additions on microstructure and mechanical properties of Al−Zn−Mg alloy welds [J]. Materials Science and Engineering A, 2007, 467: 132−138.

[7] PENG Z W, LI J F, SANG F J, CHEN Y L, ZHANG X H, ZHENG Z Q, PAN Q L. Structures and tensile properties of Sc-containing 1445 Al−Li alloy sheet [J], Journal of Alloys and Compounds, 2018, 747: 471−483.

[8] MUKHOPADHYAY A K, KUMAR A, RAVEENDRA S, SAMAJDAR I. Development of grain structure during superplastic deformation of an Al−Zn−Mg−Cu−Zr alloy containing Sc [J]. Scripta Materialia, 2011, 64: 386−389.

[9] BOMMAREDDY A, QUADIR M Z, FERRY M. Time and temperature regime of continuous grain coarsening in an ECAP-processed Al (0.1 wt. % Sc) alloy [J]. Journal of Alloys and Compounds, 2012, 527: 145−151.

[10] JIA M, ZHENG Z Q, GONG Z. Microstructure evolution of the 1469 Al−Cu−Li−Sc alloy during homogenization [J]. Journal of Alloys and Compounds, 2014, 614: 131−139.

[11] ZAKHAROV V V. Special features of crystallization of scandium-alloyed aluminum alloys [J]. Metal Science and Heat Treatment, 2012, 53: 414−419.

[12] ROYSET J, RYUM N. Scandium in aluminium alloys [J]. International Materials Reviews, 2005, 50: 19−44.

[13] LEE S L, WU C T, CHEN Y D. Effects of minor Sc and Zr on the microstructure and mechanical properties of Al−4.6Cu−0.3Mg−0.6Ag alloys [J]. Journal of Materials Engineering and Performance, 2015, 24: 1165−1172.

[14] TESLYUK M Y, PROTASOV V S. The crystal structure of ternary phases in the Sc−Cu−Al system [J]. Expert Systems with Applications, 1966, 36: 4331−4337.

[15] KHARAKTEROVA M L, ESKIN D G, TOROPOVA L S. Precipitation hardening in ternary alloys of the Al−Sc−Cu and Al−Sc−Si systems [J], Acta Metallurgica ET Materialia, 1994, 42: 2285−2290.

[16] KHARAKTEROVA M L. Phase composition of aluminum−copper−scandium alloys at 450 and 500 °C [J]. Metally, 1991, 4: 191−194.

[17] GAZIZOV M, TELESHOV V, ZAKHAROV V, KAIBYSHEV R. Solidification behavior and the effects of homogenisation on the structure of an Al−Cu−Mg−Ag−Sc alloy [J]. Journal of Alloys and Compounds, 2011, 509: 9497−9507.

[18] BURKHARDT F, SKELA B, DANEU N, SAMARDZIJA Z, STURM S, GAUDRY E, KOBE S, DUBOIS J M. A new complex ternary phase in the Al−Cr−Sc push-pull alloy [J]. Journal of Alloys and Compounds, 2018, 768: 230−239.

[19] SINGH V, PRASAD K S, GOKHALE A A. Effect of minor Sc additions on structure, age hardening and tensile properties of aluminium alloy AA8090 plate [J]. Scripta Materialia, 2004, 50: 903−908.

[20] CHEN Z G, ZHENG Z Q. Microstructural evolution and ageing behaviour of the low Cu: Mg ratio Al−Cu−Mg alloys containing scandium and lithium [J]. Scripta Materialia, 2004, 50: 1067−1071.

[21] ZHANG Hai-feng, ZHENG Zi-qiao, LIN Yi, XUE Xin-li, LUO Xiao-fu, ZHONG Jin. Effects of small addition of Sc on microstructure and properties of 2099 Al−Li alloy [J]. Journal of Central South University (Science and Technology), 2014, 45: 1420−1427. (in Chinese)

[22] MA J, YAN D S, RONG L J, LI Y Y. Effect of Sc addition on microstructure and mechanical properties of 1460 alloy [J]. Progress in Natural Science-Materials International, 2014, 24: 13−18.

[23] DUTKIEWICZ J, SIMMICH O, SCHOLZ R, CIACH R. Evolution of precipitates in AlLiCu and AlLiCuSc alloys after age-hardening treatment [J]. Materials Science and Engineering A, 1997, 234: 253−257.

[24] JIA M, ZHENG Z Q, LUO X F. Influence of AlCuSc ternary phase on the microstructure and properties of a 1469 alloy [J]. Materials Science Forum, 2014, 794−796: 1057−1062.

[25] ZHU R H, LIU Q, LI J F, XIANG S, CHEN Y L, ZHANG X H. Dynamic restoration mechanism and physically based constitutive model of 2050 Al−Li alloy during hot compression [J]. Journal of Alloys and Compounds, 2015, 650: 75−85.

[26] LEQUEU P H, SMITH K P, DANIELOU A. Aluminum−copper−lithium alloy 2050 developed for medium to thick plate [J]. Journal of Materials Engineering and Performance, 2010, 19: 841−847.

[27] YOSHIMURA R, KONNO T J, ABE E, HIRAGA K. Transmission electron microscopy study of the early stage of precipitates in aged Al−Li−Cu alloys [J]. Acta Materialia, 2003, 51: 2891−2903.

[28] YOSHIMURA R, KONNO T J, ABE E, HIRAGA K. Transmission

electron microscopy study of the evolution of precipitates in aged Al−Li−Cu alloys: the θ′ and T1 phases [J]. Acta Materialia, 2003, 51: 4251−4266.

[29] LI Jin-feng, CHEN Yong-lai, ZHANG Xu-hu, YAO Yong, ZHOU Hua. Influence of Cu and Li contents on mechanical properties and microstructures of Mg-, Ag- and Zn-microalloyed Al−Li alloys [J]. Aerospace Materials & Technology, 2015: 24−28. (in Chinese)

[30] LI Jin-feng, LIU Ping-li, CHEN Yong-lai, ZHANG Xu-hu, ZHENG Zi-qiao. Microstructures and mechanical properties of Mg, Ag and Zn mult-microalloyed Al−(3.2−3.8)Cu−(1.0−1.4) Li alloys [J]. Transactions of Nonferrous Metals Society of China, 2015, 25: 2103−2112.

[31] YIN Z M, PAN Q L, ZHANG Y H, JIANG F. Effect of minor Sc and Zr on the microstructure and mechanical properties of Al−Mg based alloys [J]. Materials Science and Engineering A, 2000, 280: 151−155.

[32] NORMAN A F, PRANGNELL P B, MCEWENB R S. The solidification behavior of dilute aluminium-scandium alloys [J]. Acta Materialia, 1998, 46: 5715−5732.

[33] ZAKHAROV V V. Effect of scandium on the structure and properties of Aluminum alloys [J]. Metal Science and Heat Treatment, 2003, 45: 246−253.

[34] PEARSON W. Lattice spacings and structures of metals and alloys [M]. Vols. 1 and 2. Oxford: Pergamon Press, 1958.

[35] BO H, LIU L B, JIN Z P. Thermodynamic analysis of Al−Sc, Cu−Sc and Al−Cu−Sc system [J]. Journal of Alloys and Compounds, 2010, 490: 318−325.

[36] YANG G, ZHANG P, SHAO D, WANG R H, CAO L P, ZHANG J Y, LIU G, CHEN B A, SUN J. The influence of Sc solute partitioning on the microalloying effect and mechanical properties of Al−Cu alloys with minor Sc addition [J]. Acta Materialia, 2016, 119: 68−79.

[37] SINGH V, PRASAD K S, GOKHALE A A. Effect of minor Sc additions on structure, age hardening and tensile properties of aluminium alloy AA8090 plate [J]. Scripta Materialia, 2004, 50: 903−908.

[38] RAGHAVAN V. Al−Cu−Sc (aluminum−copper−scandium) [J]. Journal of Phase Equilibria and Diffusion, 2010, 31: 554−555.

[39] SHI C C, ZHANG L, WU G H, ZHANG X L, CHEN A T, TAO J S. Effects of Sc addition on the microstructure and mechanical properties of cast Al−3Li−1.5Cu−0.15Zr alloy [J]. Materials Science and Engineering A, 2017, 680: 232−238.

微量 Sc 添加对 2070 铝锂合金显微组织演变和力学性能的影响

刘丹阳[1]，汪洁霞[1]，李劲风[1,2]

1. 中南大学 材料科学与工程学院，长沙 410083；
2. 中南大学 轻质高强结构材料重点实验室，长沙 410083

摘 要：通过力学测试、SEM、EPMA 和 TEM 对基于 Al−3.35Cu−1.2Li−0.4Mg−0.4Zn−0.3Mn−0.1Zr(质量分数，%)的含 Sc 和不含 Sc 两种合金的显微组织和力学性能进行研究。研究发现，0.082% (质量分数)Sc 元素的添加可形成富含 Cu 和含 Sc 的 Al_3(ScZr)粒子和 *W* 相颗粒。Al_3(ScZr)粒子可以抑制固溶过程中的再结晶和再结晶晶粒长大；而 *W* 相在固溶过程中不易溶解，可使 Cu 在固溶基体中含量减少，导致在 T8 时效过程中的含 Cu 的主强化相 T_1(Al_2CuLi)和 θ' (Al_2Cu)的分数下降。由于 *W* 相的形成，少量 Sc 的添加导致力学性能下降。

关键词：铝锂合金；Sc 添加；显微组织；力学性能

(Edited by Bing YANG)